Influence of bismuth on the solidification of Sn-0.7Cu-0.05Ni-xBi/Cu joints

S.A. Belyakov[1*], J. Xian[1], K. Sweatman[2], T. Nishimura[2], T. Akaiwa[2], C.M. Gourlay[1]

[1] Department of Materials, Imperial College, London. SW7 2AZ. UK

[2] Nihon Superior Co., Ltd., NS Building, Suita 564-0063, Japan

Abstract

The improvement of solder joint mechanical performance due to bismuth additions is of ongoing interest. This paper investigates the influence of 0 – 14wt% Bi on microstructure formation in Sn-0.7wt%Cu-0.05wt%Ni-xBi solder balls on Cu substrates. It is shown that Bi additions reduce the Ni content of $(Cu,Ni)_6Sn_5$, increase the size of primary $(Cu,Ni)_6Sn_5$ rods and reduce the thickness of the Cu_6Sn_5 reaction layer, although these effects are subtle until the Bi content reaches ~5wt%Bi and Bi additions of ≤5wt% did not significantly affect the positive effects of Ni. Higher Bi additions (≥8wt% Bi) caused a transition of the tin growth texture from columnar grains with a <110> fibre texture towards a single grain with subgrains. Bi additions increased the non-equilibrium freezing range and caused a nonequilibrium ternary eutectic reaction in joints containing ≥2wt% Bi. Bi contents less than 2wt% are required to prevent (Bi) phase formation during solidification

Key words: *intermetallics; microstructure; phase diagrams; thermal analysis; Lead-free solder*

1 Introduction

Sn-Cu-Ni solders have been used in electronics since 1999 and Sn-0.7Cu-0.05Ni (wt%) has become a popular no-Ag Pb-free solder [1, 2]. It has found application as a wave and reflow solder as well as a HASL (hot-air surface levelling) surface finish. Dilute Ni additions reduce the solubility of Cu in liquid tin [3, 4], such that Sn-0.7Cu is a hypoeutectic composition (in the βSn primary phase field) and Sn-0.7Cu-0.05Ni is in the Cu_6Sn_5 primary phase field [5]. 0.05wt%Ni has been found to strongly increase the ability of Sn-Cu-Ni alloys to flow as they solidify [5-7] which improves drainage and reduces bridging and icicles in wave soldering [5, 8]. Furthermore, the dilute Ni addition has been demonstrated to significantly affect the intermetallics that form during soldering. For example, Ni stabilises the high temperature hexagonal polymorph of Cu_6Sn_5 at low temperature [9, 10], and Sn-0.7Cu-0.05Ni/Cu joints have a fine-grained $(Cu,Ni)_6Sn_5$ interfacial layer [11, 12] and suppressed growth of the Cu_3Sn interfacial layer [11, 13-16]. It has been further demonstrated that additions of Ni to Sn-0.7Cu solder result in considerable refinement of the Cu_6Sn_5 primary crystals in the solder bulk, decreasing their size and increasing their number density [17]. Sn-0.7Cu-0.05Ni has been shown to have higher compliance [1] and higher impact strength [18] compared with high-silver Sn-Ag-Cu (SAC) solders which is important in applications that experience drop impacts. However, Sn-0.7Cu-0.05Ni has lower creep strength and fatigue life in thermal cycling than high-silver SAC solders [19-24]. Therefore, there is interest in developing Sn-Cu-Ni-based solders with improved thermal cycling performance without adding Ag. To this end, Bi additions to Sn-0.7Cu-0.05Ni are being pursued and have shown promising results in both shear impact and thermal cycling performance. However, there has been little research on the microstructure of Sn-Cu-Ni-Bi solders and there is little understanding of how the Bi addition interacts with the positive effects of Ni.

In contrast, there has been substantial research on Bi additions to Sn-Ag-Cu solders (typically in the range of 0-4wt%Bi) and a number of advantages have been reported. The research has demonstrated that Bi additions to SAC alloys improve their mechanical performance, increasing solder joint shear

strength [25-28], thermal fatigue resistance [29] and improve the drop-impact performance [29]. This is reportedly due to solid solution strengthening of βSn with Bi and/or precipitation strengthening with (Bi) phases [25, 28, 30-32]. Additionally, Bi additions have been shown to improve wetting and spreading of lead-free solders [27, 29, 33] and to lower their liquidus temperature [34]. Furthermore, Bi additions to SAC solders hinder the growth rate of the Cu_3Sn interfacial IMC layer [29, 35, 36] and to reduce the propensity to whisker growth [37, 38].

Since the influence of Bi on Sn-Cu-Ni/Cu solder reactions has not been studied in detail, the current investigation was undertaken to explore IMC layer formation, the solidification path and the formation of the bulk solder microstructure during soldering of Sn-0.7Cu-0.05Ni-xBi/Cu joints. Our focus is on how Bi and Ni alter the phase equilibria and predicted solidification path, how the Bi additions affect the βSn grain structure (i.e. the number of orientations and the growth texture), and on the formation of (Bi) phase through a non-equilibrium eutectic reaction. We study a wide range of Bi contents from 0-14wt%Bi, spanning compositions that would be (i) solid solution strengthened and (ii) both solid solution and precipitation strengthened by Bi.

2. Methods

All compositions in this paper are in wt% unless otherwise stated. Sn-0.7Cu and Sn-0.7Cu-0.05Ni-xBi (where x = 0, 1.5, 2, 5, 8, 10 and 14 wt%) alloys were prepared from commercial purity (CP) materials by mixing the required amount of a Sn-10wt%Ni, Sn-10wt%Cu master alloys and 99.9Bi% with ~150g of 99.9%Sn in a graphite crucible and heating in a resistance furnace to 450°C. After 1-hour holding, the melt was stirred with a preheated graphite rod and cast into a stainless steel mould coated in BN. The solder compositions, measured by XRF spectroscopy, are given in Table 1. The ingots were then rolled to 30μm foils. 500±20μm diameter solder balls were prepared by punching 1.6mm round preforms from the foils and then reflowing them with ROL1 tacky flux (by IPC J-STD-004) on a hotplate at 280°C to form spheres by the action of surface tension.

Standard FR4 Cu-OSP test boards were used as Cu substrates with 500μm circular pads. To produce solder joints, solder balls were placed on the Cu-OSP pads, fluxed with ROL1 tacky flux, and then reflowed in a LFR400HTX TORNADO reflow oven (Surface Mount Technology, Isle of Wight, UK). The thermal profile involved heating at ~2K/s to a peak temperature of ~251°C and cooling at ~3K/s to room temperature. The time above the eutectic temperature (227°C for Sn-0.7Cu-0.05Ni) was ~45s. At least 15 solder joints were soldered and analysed for each composition.

Liquidus temperatures were measured by cyclic DSC. Figure 1A illustrates the method used which is similar to that in references [39, 40]. First, a ~300mg sample was heated at 10 K/min to a temperature where a mixture of liquid and solid βSn are known to co-exist, then it was held isothermally for 30 min, then heated to 250°C at 10K/min and cooled to 180°C at 10K/min ending the cycle. The next cycle involved isothermal holding at a temperature 0.5K higher than the previous cycle (as shown in Figure 1A). If, on heating after the isothermal holding, an endothermic peak was detectable (curves 1-6 in Figure 1A), some βSn was present before the isothermal hold which was defined as being below the liquidus temperature. When no endothermic peak was found on heating after isothermal holding (curves 7-9 in Figure 1A), the sample had completely melted at the isothermal holding temperature,

which was defined as being above the liquidus temperature. The liquidus was defined as the median isothermal holding temperature in curves 6 and 7 in Figure 1A. This method provided an accuracy of 0.25K for βSn liquidus temperature determination.

To test for any small fraction of intermetallic compounds present prior to the DSC-measured 'liquidus' temperature, isothermal holding experiments were carried out on ~8g samples in Ø=4mm sealed quartz tubes held vertically at 250°C for 24 hours. After the experiment, samples were quenched in water. If present, the low fraction of intermetallic particles settled to produce a sedimented layer on the bottom of the sample. The compositions of the intermetallics were then studied by SEM-EDX.

In order to determine the equilibrium solidus temperatures, samples were first homogenised at 130°C for up to 1400hours, to avoid any composition gradients (coring) and to dissolve any nonequilibrium eutectic (Bi). Figure 1B illustrates representative examples of DSC heating curves in the as-solidified and equilibrated conditions. The equilibrated sample provides a much sharper onset and a higher onset temperature. The solidus temperature was then defined as the temperature of the first departure from the baseline on heating in homogenised samples. Note that this method is preferred to the linear extrapolation method when studying solid solution alloys [41].

For measurement of nucleation undercooling in Sn-0.7Cu-0.05Ni-xBi 500µm solder balls or solder joints, 5-6 samples were cycled in the range of 180-240°C, ten times each. Nucleation undercooling was then defined as the difference between the liquidus temperature (measured by cyclic DSC) and the first onset on cooling in the DSC curves.

All samples were mounted in Struers VersoCit acrylic cold mounting resin and wet ground to 2400 grit SiC paper followed by polishing with colloidal silica. For the investigation of the three-dimensional morphology of intermetallic phases and interfacial IMC layers, some solder joints were selectively etched with a solution of 5% NaOH and 3.5% orthonitrophenol in distilled H_2O. Specimens were immersed in the etchant at 60 °C for 1-15 min.

Analytical scanning electron microscopy (SEM) was conducted on a Zeiss AURIGA field-emission gun-SEM (Carl Zeiss, Oberkochen, Germany) equipped with an Oxford Instruments INCA x-sight energy dispersive x-ray (EDX) detector (Oxford Instruments, Oxfordshire, UK) and a Bruker electron backscatter diffraction (EBSD) detector (Bruker AXS Inc., Fitchburg, WI).

The average interfacial IMC layer thickness was determined by calculating the area of the Cu_6Sn_5 crystals at the interface and then dividing by the length of the layer. At least five SEM micrographs from different areas were analysed. The width of the analysed area in each case was 30μm. The average grain size of Cu_6Sn_5 scallops was measured from above after selective removal of βSn by calculating the average number of Cu_6Sn_5 scallops per unit area and then converting it into average grain size using ASTM E112-12 standard. At least five SEM micrographs from different areas were analysed.

3 Results and Discussion

3.1 Influence of Ni and Bi on the phase equilibria of bulk solders.

DSC measurements of liquidus and solidus temperatures in the Sn-0.7Cu-0.05Ni-xBi alloys are summarized in Table 2 and plotted in Figure 2A. The lines drawn through the Sn-0.7Cu-0.05Ni-xBi points in Figure 2A are best-fit linear curves to our data and the red lines are the binary Sn-Bi phase diagram calculated by NIST [42]. It can be seen that the addition of 0.7Cu and 0.05Ni results in an almost uniform drop of the βSn liquidus line by ~4K and solidus line by ~8K relative to the binary Sn-Bi system in [42]. As expected, the freezing range increases with Bi additions and, in Sn-Cu-Ni-Bi alloys, it occurs at a rate similar to that in the binary Sn-Bi system; the Bi partition coefficients, $k^{Bi} = C_S^{Bi}/C_L^{Bi}$, are similar in both the binary and quaternary systems, with k = 0.31 in binary Sn-Bi and k^{Bi} = 0.28 in Sn-Cu-Ni-Bi. Our experimental results are significantly different to those in ThermoCalc database TCSLD 3.1 [43] where the liquidus data are similar but the solidus line is much steeper, giving much lower values for the Bi partition coefficient of k^{Bi} ~0.13.

Figure 3 shows the results of quenched Sn-Cu-Ni-Bi samples that had been held at 250°C for 192 hours. The Sn-0.7Cu samples contained no discernable particles at the top or bottom of the sample at 250°C, as expected. In contrast, all Sn-0.7-0.05Ni-xBi solders contained an obvious layer of particles that settled under gravity at 250°C (Figure 3). These were determined to be $(Cu,Ni)_6Sn_5$ by SEM-EDX (Table 3). Previous work has shown that Sn-0.7Cu-0.05Ni lies in the Cu_6Sn_5 primary phase field [3, 5, 44] and Figure 3 shows that Sn-0.7Cu-0.05Ni-xBi containing 0-14wt%Bi also lie in the $(Cu,Ni)_6Sn_5$ primary phase field. Thus, the true liquidus temperature of the Ni-containing alloys is more than 250°C, and the 'liquidus' temperature measured by DSC is the equilibrium βSn-Cu_6Sn_5 eutectic start temperature. The primary $(Cu,Ni)_6Sn_5$ were not detected by DSC due to the small heat flux associated with a very low fraction of $(Cu,Ni)_6Sn_5$ forming over a wide temperature range. With this information, a vertical section through (99.25-x)Sn-0.7Cu-0.05Ni-xBi can be deduced for the composition and temperature range studied and is plotted in Figure 2B.

Table 3 shows that the concentration of Ni in $(Cu,Ni)_6Sn_5$ at 250°C (from samples similar to Figure 3) decreases with increasing Bi content, from ~17 at%Ni at 0Bi to 8at%Ni with 14wt%Bi.

Figure 4A shows the equilibrium and Scheil solidification paths predicted using ThermoCalc database TCSLD v3.1 for Sn-0.7Cu-0.05Ni-5Bi. There is a difference between the ThermoCalc prediction and our measured solidus temperature (Table 2) which is due to the binary Sn-Bi data used in the assessment of ThermoCalc TCSLD v3.1 as discussed earlier with Figure 2. Despite this, Figure 4A shows the key features of the solidification path in Sn-0.7Cu-0.05Ni-xBi solders and the role played by diffusion in the solid. A small fraction (~1.2 mole% or ~1.1 mass%) of primary $(Cu,Ni)_6Sn_5$ is predicted to exist in the liquid at 250°C, in agreement with Figure 3. On cooling, a small increase in the mass% of primary $(Cu,Ni)_6Sn_5$ is predicted before a L → βSn+$(Cu,Ni)_6Sn_5$ eutectic reaction with a freezing range that depends on the degree of backdiffusion in the solid phases. In the limit of infinite diffusion (full equilibrium), the eutectic reaction ends at the solidus temperature and no (Bi)-containing eutectic forms. In the limit of zero diffusion in the solid (the Scheil assumption), the eutectic reaction continues to ~138°C and ~4.5mol% (~5.6 mass%) of βSn+$(Cu,Ni)_6Sn_5$+(Bi) eutectic is predicted. Figure 4B shows the Scheil solidification paths predicted using ThermoCalc TCSLD v3.1 for all compositions in this study. It can be seen that, with increasing Bi content, the freezing range of the βSn+$(Cu,Ni)_6Sn_5$ eutectic increases and the fraction of non-equilibrium ternary eutectic increases (and so the fraction of (Bi) phase increases). Note that, since the partition coefficient, k^{Bi}, is lower in TCSLD v3.1 than in our measurements, Figure 4B is an overprediction of the fraction of ternary eutectic formed during Scheil solidification.

During soldering on Cu substrates, Cu dissolution will increase the Cu content in the liquid so that all solder compositions are in the Cu_6Sn_5 primary phase field [17]. The predicted solidification path for six solders after Cu dissolution are plotted as dashed in Figure 4B. It can be seen that dissolution of Cu into the liquid solder does not strongly influence the predicted solidification paths for the Sn-0.7Cu-0.05Ni-xBi/Cu joints.

Figure 4A and B predict that all compositions of this study should solidify with primary Cu_6Sn_5, and $\beta Sn+Cu_6Sn_5$ eutectic, and non-equilibrium $\beta Sn+(Cu,Ni)_6Sn_5+(Bi)$ eutectic formation is expected to depend on the degree of diffusion in the solid. It will be seen in the remainder of this paper that the microstructures are more complex than this due to kinetic factors such as the nucleation undercooling for βSn and the competitive growth kinetics between βSn dendrite tips and a eutectic front during growth in an undercooled melt.

3.2 Influence of Ni and Bi on the IMC layer and bulk (primary) IMC particles in joints on Cu

Figure 5 compares representative cross sections of the Cu_6Sn_5 layer in Sn-0.7Cu/Cu and Sn-0.7Cu-0.05Ni-xBi/Cu joints in the 'as-soldered' condition. Note that the βSn matrix has been slightly etched to improve visualization of the IMC layer microstructures. It can be seen that there is a marked difference between Sn-0.7Cu/Cu and Sn-0.7Cu-0.05Ni/Cu joints; the addition of 0.05wt%Ni significantly decreases the Cu_6Sn_5 scallop grain size (quantified in Figure 6B) and produces a more dense and uniform IMC layer (Figure 5), consistent with previous research [17, 45].

Additions of Bi to Sn-0.7Cu-0.05Ni affected the layer thickness and the size of the $(Cu,Ni)_6Sn_5$ scallops as can be seen from Figures 5 and 6. From Figure 6A, it can be seen that the IMC layer thickness decreases with increasing Bi content: from ~2.3μm for Sn-0.7Cu-0.05Ni to 1.7μm when 14wt%Bi was added to the alloy. This observation is consistent with previous results reported for Cu_6Sn_5 IMC layers in Sn-Ag-xBi (x = 0,1,2,3 and 4) soldered on Cu substrates [36] where the authors demonstrated a decrease in Cu_6Sn_5 growth constant in the liquid and solid state when Bi was added to the solder. Solubility of Cu is expected to decrease with Bi additions and this in turn will slow the reaction rate between the molten solder and the Cu substrate affecting the thickness of the interfacial IMC layer [36]. Additionally, as Bi is not soluble in Cu_6Sn_5, it is rejected from the Cu_6Sn_5 reaction front into the molten solder during IMC layer growth and the Bi concentration build up slows IMC layer growth [36]. It was found that reflow profiles with higher peak temperatures exaggerate the effects of Bi on IMC layer thickness. For instance, there is a limited difference between alloys when the peak reflow

temperature was ~238°C and there is a more significant decrease of the IMC layer thickness with Bi content when the peak reflow temperature was ~250°C (Figure 6A).

Figure 6B quantifies the size (width) of the interfacial $(Cu,Ni)_6Sn_5$ IMC scallops shown in Figure 5. It can be seen that (i) addition of 0.05wt%Ni to Sn-0.7Cu refines the $(Cu,Ni)_6Sn_5$ scallops, decreasing their average diameter from ~2µm to ~1µm and (ii) Bi additions to Sn-0.7Cu-0.05Ni cause a gradual increase in $(Cu,Ni)_6Sn_5$ scallop size from about 1µm for Sn-0.7Cu-0.05Ni to 1.4µm when 14wt%Bi is added to the solder.

Figure 7 compares representative images of primary $(Cu,Ni)_6Sn_5$ crystals formed in the bulk solder of Sn-0.7Cu/Cu and Sn-0.7Cu-0.05Ni-xBi/Cu joints. There is a marked difference between Sn-0.7Cu/Cu and Sn-0.7Cu-0.05Ni/Cu joints; Sn-0.7Cu/Cu solder joints typically form long hexagonal Cu_6Sn_5 rods during solidification, sometimes spanning the whole cross section of the 500µm solder ball. These long Cu_6Sn_5 rod-like crystals were frequently observed to have hollow cores. Similar results for Sn-0.7Cu/Cu solder joints were also shown previously in [46-50]. The 0.05wt%Ni addition to Sn-0.7Cu strongly reduced the size (from ~100-150µm to ~10µm) and increased the number density of primary Cu_6Sn_5 IMC crystals in the solder bulk, consistent with [17]. The difference between Sn-0.7Cu/Cu and Sn-0.7Cu-0.05Ni/Cu can be seen from the 2D sections in Figure 7A, the protruding rods in the partially-etched balls of Sn-0.7Cu/Cu in Figure 7B and the typical examples of extracted primary IMCs in Figure 7C and D (noting the different scale bars in Figure 7C and D). A further difference is that primary Cu_6Sn_5 in Sn-0.7Cu-0.05Ni/Cu solder joints (Figure 7D) tend to have a more complex morphology, similar to the "X-shape" crystals described in [50].

Addition of Bi to Sn-0.7Cu-0.05Ni/Cu solder joints of up to 5wt% were not found to influence the size and morphology of $(Cu,Ni)_6Sn_5$ primary crystals significantly. However, when 8wt% or 14wt%Bi were added to the solder, the size of primary $(Cu,Ni)_6Sn_5$ increased up to ~100µm for Sn-0.7Cu-0.05Ni-14Bi/Cu (Figure 7E). Typical $(Cu,Ni)_6Sn_5$ crystals formed in high-Bi solders preserved the complex "X-shape".

SEM-EDX composition data for the interfacial IMC layers and bulk (primary) IMCs are summarized in Table 4. Regardless of the amount of Bi added to Sn-0.7Cu-0.05Ni solder (up to 14wt%) there is no detectable solubility for Bi in the $(Cu,Ni)_6Sn_5$ phase. Ni levels in $(Cu,Ni)_6Sn_5$ were found to decrease with increasing Bi additions (Table 4). This might be partially associated with the observed increase of volume fraction of bulk $(Cu,Ni)_6Sn_5$ in high-Bi solders (i.e. Figure 7), whilst the amount of Ni in the solder joint system remains constant. A similar decreasing Ni-content in $(Cu,Ni)_6Sn_5$ with increasing Bi trend was measured for the interfacial $(Cu,Ni)_6Sn_5$ layers, however, the interfacial $(Cu,Ni)_6Sn_5$ contained half or less Ni compared to the bulk $(Cu,Ni)_6Sn_5$ phase (Table 4). Note that, even with 14wt%Bi, the Ni level in the $(Cu,Ni)_6Sn_5$ layer is more than 2at%, which has been shown to be sufficient to stabilise the 'high temperature' hexagonal polymorph of Cu_6Sn_5 at low temperature [51].

Comparing Table 3 with Table 4, it can be seen that the $(Cu,Ni)_6Sn_5$ in joints on Cu substrates contains significantly less Ni than in $(Cu,Ni)_6Sn_5$ when the bulk solder is solidified (without a substrate). This shows the importance of the Cu dissolved from the substrate in changing the liquid composition.

3.3 Influence of Bi additions on nucleation undercooling for βSn

DSC measurements of the nucleation undercooling of βSn in 500±20μm freestanding solder balls and joints gave a large scatter in the nucleation undercooling for all compositions. The mean undercooling for Sn-0.7Cu-0.05Ni balls was ~38K, similar to reference [52]. Additions of Bi to the solder did not influence the βSn nucleation undercooling in a distinct manner. In all cases, the nucleation undercooling of βSn was relatively high and variable and the addition of 0.05wt%Ni or 1.5-14wt%Bi to Sn-0.7Cu did not have any clear influence on the undercooling. We note that this is in contrast to various other additions, such as Zn [53, 54], Al [53], Mn [55], Ti [55], Pt or Pd [56] or Co [54, 57] which strongly reduce the βSn nucleation undercooling in Sn-Cu, Sn-Ag and Sn-Ag-Cu solders.

βSn nucleation undercooling was decreased by about 10-20K when soldering to a Cu substrate for all solder compositions studied, but this still resulted in considerable values of undercooling of 20-30K in solder joints. This result is consistent with various studies that have shown that the nucleation

undercooling is often lower when soldering on Cu substrates than in freestanding balls [52, 58-60] and we discuss the influence of the Cu_6Sn_5 layer on the nucleation of tin in detail in [61].

3.4 βSn grain structures in Sn-0.7Cu/Cu and Sn-0.7Cu-0.05Ni-xBi/Cu

Figure 8 summarizes representative βSn grain structures (EBSD IPF-X maps) formed in Sn-0.7Cu/Cu and Sn-0.7Cu-0.05Ni-xBi/Cu solder joints. 15-20 samples of each composition were analysed and Figure 8 shows four typical examples for each composition.

The number of grains was measured in each cross-section using the EBSD IPF maps, pole figures and grain-grain misorientations. We defined independent grains as grains not related by any 'special' boundary i.e. 57.2° and 62.8° twins @[010] or any coincidence site lattice boundaries (such as 22.3° @[110]; 43° @[010]; 71° @[010]) [62]; we also excluded low angle grain boundaries (<15°) as well as any grains smaller than 50 μm and any deformation twins. The data are plotted in Figure 9 where it can be seen that for Sn-0.7Cu-0.05Ni-xBi/Cu joints with Bi additions of up to 5wt% Bi, each cross-section contained 5-8 independent βSn grains. There was no strong evidence for solidification twinning, which suggests there were multiple nucleation events in the solder joints. It can be seen in Figures 8 and 9 that the 0.05wt%Ni additions and Bi additions up to ~5wt%Bi caused only subtle changes in the βSn grain structures compared with Sn-0.7Cu/Cu joints. A further increase in Bi level to ~8wt%Bi and higher resulted in a gradual change of solder joint microstructure towards one βSn grain that often had a range of low angle grain boundaries across the joint (Figure 8 and 9).

As can be seen in Figure 8, the joints with up to 5wt%Bi solidified with near-columnar growth of βSn from the Cu_6Sn_5 layer. Figure 10 shows this in more detail for a typical Sn-0.7Cu-0.05Ni/Cu joint. βSn unit cell orientations are superimposed on an EBSD IPF-X map, and <110> and <001> pole figures are shown for the region just above the Cu_6Sn_5 layer and the region at the top of the solder ball in Figure 10B. It can be seen that there is a wide variety of randomly oriented βSn grains near the solder-substrate interface and a decreasing number further into the bulk. Each orientation that developed into a much larger βSn grain is consistent with <110> growth from the Cu_6Sn_5 reaction layer. βSn grains

that nucleated with unfavourable orientations, i.e. with all <110> directions oriented close to the horizontal plane (Figure 10), were outcompeted by those growing with one of [110] or [1-10] close to the y-direction, into the bulk liquid. The pole figures in Figure 10B confirm the grain selection by competitive growth. It can be seen that a large number of random βSn grain orientations in the vicinity of the interfacial area evolves into a preferred <110> texture by the end of growth near the top surface. Figure 10C shows βSn pole figures for the upper parts of Sn-0.7Cu/Cu, Sn-0.7Cu-0.05Ni-1.5Bi/Cu and Sn-0.7Cu-0.05Ni-5Bi/Cu joints. Each has a similar strong <110> growth texture, showing that the growth competition and <110> growth of βSn is not strongly influenced by the Ni or Bi additions (up to ~5wt% Bi).

Therefore, a feature of Sn-0.7Cu-0.05Ni-xBi (x≤5) alloys is that there is a relatively fine-grained and non-textured region of βSn near the Cu substrate and a reproducible <110> texture away from the Cu substrate. Note that this is significantly different to joints made with Ag-containing solders on Cu substrates (e.g. SAC or SnAg solders), where there is usually only a single nucleation event and either single grain, cyclically twinned 'beachball', or interlaced twinned structures [52, 63-67] and no reproducible grain orientation relative to the substrate [68]. In the case of Sn-0.7Cu-0.05Ni-xBi (x≤5) solders, this type of βSn grain texture where the c-axis of the βSn crystal is oriented horizontally might be favourable for retarding electromigration that occurs fastest along the c-direction in the βSn crystal [69, 70].

The Sn-0.7Cu-0.05Ni-xBi/Cu joints containing up to ~8%Bi solidified to produce a large volume fraction of βSn dendrites, even though these solder compositions are in the Cu_6Sn_5 primary phase field (Figure 2B). Similarly, Sn-0.7Cu/Cu joints solidified with a high fraction of βSn dendrites despite being a hypereutectic composition after Cu substrate dissolution. For example, the typical bulk microstructure in Sn-0.7Cu/Cu solder joints is overviewed in Figure 11 where an EBSD IPF-x map is superimposed on a shallow etched SEM image to highlight how the βSn orientations correspond to the dendrites and eutectic. One columnar dendrite is selected in Figure 11D with its unit cell

orientation superimposed. It can be seen that the growth directions and branching directions are close to <110>. The secondary dendrite arm spacing is significantly smaller close to the Cu_6Sn_5 layer than further in the bulk (Figure 11D) which suggests that the velocity of the dendrite tip was highest (and the solidification time was shortest) near the IMC layer. This is further evidence that βSn nucleated on/near the Cu_6Sn_5 layer because, after a large nucleation undercooling, the initial growth occurs at highest tip undercooling and then tip growth decelerates as the release of latent heat reduces the βSn dendrite tip growth undercooling [71]. Figure 11F quantifies the secondary dendrite arm spacing shown in Figure 11D. It can be seen that the spacing increased from a value of less than 1μm in the vicinity of the interface to ~9μm at the maximum growth distance close to the surface of the solder ball.

Occasionally, the columnar grains in Figure 8 were βSn-Cu_6Sn_5 eutectic grains. An example is shown in Figure 12 for a Sn-0.7Cu/Cu joint. After etching, it can be seen that the columnar blue grain marked with an 'X' in the EBSD map (Figure 12A) is a βSn-Cu_6Sn_5 eutectic grain with Cu_6Sn_5 rods aligned with the growth direction and fanning out, indicating that this was eutectic cell growth (similar to that in unidirectional solidification experiments [44]) The presence of βSn dendrites with interdendritic eutectic in most samples and eutectic grains in a few samples (of the same composition) is most likely due to the variation in βSn nucleation undercooling from joint to joint and the resulting difference in growth competition between a eutectic front and a βSn dendrite front.

As can be seen in Figures 8, 10 and 11, many of the columnar grains in the EBSD maps are made up of multiple similarly-coloured subregions that all emanate from a similar point on/near the Cu_6Sn_5 layer. For example, in Figure 11C, the region labelled 'grain 3' consists of different shades of blue. Each subregion has a near-uniform orientation (shade of blue) and there are sharp changes of orientation between these subregions as shown in Figure 11E. Some of these had a range of misorientations up to 30-35° within what appears to be the same grain. In contrast, the Ni and ≤5% Bi additions resulted in less frequent formation of such regions (Figure 8).

Bi additions of 8wt% and higher started to change the typical columnar βSn grain structure of Sn-0.7Cu-0.05Ni alloys towards single grain solder joints. For example, as shown in Figure 8, with 8% Bi, some joints have columnar grains whereas others are approximately a single βSn grain. Figure 13 shows 'single' grain solder joints with 8 and 10wt%Bi in more detail. There is a gradual misorientation gradient from one side of the solder balls to the other with a high total misorientation of >40° made up of 4-5 smaller misorientation changes each less than 20°. Detailed analysis of the EBSD data showed that there were no reproducible or special angles for βSn grain boundary misorientation such as the coincidence site lattice boundaries discussed in [62]. One dominant colour in EBSD maps in Figure 13 suggests a single nucleation event in these joints and the 0-20° subgrains are likely to develop during βSn growth similar to the distinct subregions within single βSn grains discussed earlier for Sn-0.7Cu-0.05Ni-xBi/Cu joints (where x≤5). As there is no grain selection by competitive growth in solders containing 8-10wt%Bi (i.e Figure 13), no reproducible βSn grain orientation was observed with respect to the solder/substrate interface.

Joints containing more than 10wt% Bi also contained approximately a single-grain with gradual misorientations but also developed recrystallized grains within a few hours of soldering. This phenomenon will be discussed in a separate publication.

Figure 14 compares typical bulk microstructures of Sn-0.7Cu-0.05Ni-xBi/Cu solder joints containing 0, 1.5, 8 and 14wt%Bi, where the βSn matrix has been shallow etched for better visualization of βSn dendrites and βSn-Cu_6Sn_5 eutectic regions. As can be seen in the magnified regions in Figure 14.

, joints with up to 8wt% Bi (i.e. Figure 14C) consisted of βSn dendrites with interdendritic eutectic. In Sn-0.7Cu-0.05Ni-14Bi/Cu joints (Figure 14D), the bulk microstructure contained no discernible βSn dendrites. Instead, there was a cell-like structure (i.e. Figure 14D) featuring multiple randomly oriented βSn grains.

Increasing Bi levels (≥8wt%) affected the size, morphology and spacing of the Cu_6Sn_5 eutectic phase. It was found to be much coarser in Sn-0.7Cu-0.05Ni-14Bi/Cu solder joints measuring up to ~1-1.5µm

in cross-section in contrast to submicron Cu_6Sn_5 eutectic rods formed in Sn-0.7Cu-0.05Ni-xBi (x≤5) alloys (Figure 14). In past work, Bi additions of 1-2wt% were occasionally reported to refine the microstructure of solder joints refining both the size of βSn dendrites and the Cu_6Sn_5 eutectic phase in Sn-Cu [72] solder and Sn-Ag-Cu alloys [29]. In contrast, other work at similar Bi level found Bi to increase the volume fraction and size of βSn dendrites in SAC solders [26]. However, significant changes to the microstructure were not found at the 1-2wt% Bi level in present research. Furthermore, it was observed that Bi additions of up to 5wt%Bi do not cause any significant change in the size of βSn dendrites nor the volume fraction and size of Cu_6Sn_5 eutectic phase. For instance, Figure 14 clearly demonstrates that a Bi addition of 1.5wt% or even 8wt% to Sn-0.7Cu-0.05Ni solder has very little effect on microstructure refinement in solder joints. Analysis of shallow-etched SEM micrographs showed that the area fraction of βSn dendrites in solder joints is about ~30-40% for all composition studied up to 8wt%Bi. Discrepancies in the reported data might be caused by variations in the solder joint reflow conditions. For instance, as demonstrated in Figure 6A, peak reflow temperature has a significant effect on the thickness reduction of the interfacial IMC layer with increasing Bi additions.

3.5 Nonequilibrium Sn-$(Cu,Ni)_6Sn_5$-(Bi) eutectic

Figure 15 depicts examples of non-equilibrium grain boundary (Bi) due to the L → βSn + $(Cu,Ni)_6Sn_5$ + (Bi) eutectic reaction that formed in solder joints containing 5wt%Bi and 8wt%Bi. Non-equilibrium (Bi) eutectic was always observed in Sn-0.7Cu-0.05Ni-xBi/Cu solder joints containing ≥5wt%Bi, sometimes found in samples with 2wt% but it was never detected in samples with Bi additions less than 2wt%. In order to prove the non-equilibrium nature of the grain boundary (Bi) phase Figure 15D gives examples of DSC heating curves for a ~250mg sample of Sn-0.7Cu-0.05Ni-2Bi. The upper heating curve corresponds to heating the sample after a prior cooling rate of 3K/s, whereas the lower heating curve corresponds to the same sample heated after a prior cooling rate of 0.016K/s (~200 times slower than the typical cooling rate during soldering). As can be seen from Figure 15D, the peak corresponding to the ternary eutectic reaction disappears when the cooling conditions were closer to equilibrium

solidification. Similar results were obtained for Sn-0.7Cu-0.05Ni compositions containing 2-14wt%Bi. However, for higher Bi contents, some non-equilibrium (Bi) eutectic formed even after samples were cooled at 0.016K/s (Figure 15E) and only samples heat treated in the temperature range above the ternary eutectic temperature and below the solidus temperature (in Figure 2B) and then quenched provided DSC heating curves with no evidence of eutectic melting at 138°C. DSC analysis also demonstrated that that (Bi) phase has nucleation difficulties with a (Bi) nucleation undercooling of 6-25K.

Section 3.1 and Figure 4 presented the equilibrium and Scheil solidification paths predicted for Sn-0.7Cu-0.05Ni-xBi solders. As can be seen from Figure 4, under equilibrium conditions, (Bi) phase is not expected to form in a ternary eutectic reaction L → βSn-$(Cu,Ni)_6Sn_5$-(Bi) for all compositions considered in this study (0-14wt%Bi). However, using the Scheil assumption (zero diffusion in the solid phases), a small fraction of the ternary eutectic βSn-$(Cu,Ni)_6Sn_5$-(Bi) at all Bi levels is predicted, even at 1.5wt%Bi addition (Figure 4B). In reality, the minimum Bi content at which some non-equilibrium (Bi)-containing eutectic was observed in this study was 2wt% Bi. This suggests that, at the cooling rates used in the experiment of ~3K/s (which is typical for electronics manufacturing), the back-diffusion of Bi in βSn was sufficient to prevent the liquid composition from reaching the ternary eutectic point in the last stages of freezing only in alloys containing less than 2wt%Bi.

Conclusions

The influence of combined Ni and Bi additions on the solidification and microstructure of 500±20µm Sn-0.7wt%Cu-0.05wt%Ni-xBi BGA joints on Cu substrates (x=0-14wt% Bi) has been investigated. The major conclusions can be summarized as follows:

1. Sn-0.7Cu-0.05Ni-(0-14)Bi solders lie in the Cu_6Sn_5 primary phase field. A small volume fraction of $(Cu,Ni)_6Sn_5$ co-exists with liquid at 250°C.
2. Bi additions reduced the effective βSn 'liquidus' temperature with a slope of m_L = -1.3K/wt%Bi and the solidus temperature with a slope of m_s= -4.8K/wt%Bi, giving a near-constant partition coefficient for Bi in βSn of k^{Bi}= 0.28.
3. No solubility was measured for Bi in $(Cu,Ni)_6Sn_5$. Bi additions decreased the Ni concentration in $(Cu,Ni)_6Sn_5$; however, the lowest Ni level of ~2at%Ni was higher than that reportedly required to stabilise the hexagonal polymorph of Cu_6Sn_5 at low temperature.
4. The 0.05wt% Ni addition to Sn-0.7Cu/Cu solder joints reduced the size (width) of Cu_6Sn_5 scallops from ~2 to ~1µm and had little effect on the thickness of the IMC layer. Bi additions increased the size of Cu_6Sn_5 scallops and reduced the thickness of the Cu_6Sn_5 layer.
5. The 0.05wt% Ni addition to Sn-0.7Cu/Cu reduced the size of primary Cu_6Sn_5 rods in the bulk solder from >100µm to ~10µm. When the Bi content was ≥8wt%, Bi additions increased the size of primary $(Cu,Ni)_6Sn_5$ rods to ~100µm.
6. The Ni and Bi additions had no significant catalytic effect on βSn nucleation. High and variable undercoolings of ~35K ± 20K were measured in 500µm Sn-0.7Cu-0.05Ni-xBi solder balls and joints.
7. In Sn-0.7Cu-0.05Ni-xBi/Cu (where x≤5) solder joints, the βSn grain structure was columnar and grew from the Cu_6Sn_5 layer, with a relatively fine-grained and non-textured βSn region near the Cu substrate and a strong <110> texture away from the Cu substrate due to competitive βSn growth.

8. Addition of 8wt% Bi and higher to Sn-0.7Cu-0.05Ni/Cu joints caused a transition from a columnar grain structure to a single grain structure with low boundary angle subregions in the solder bulk.
9. In Sn-0.7Cu-0.05Ni-xBi/Cu (x≤8wt%), the Cu_6Sn_5 eutectic particles were submicrometre in size and not strongly affected by the Bi addition. However, Bi levels ≥8wt% resulted in considerably coarser Cu_6Sn_5 eutectic rods of ~1-2μm.
10. All compositions studied here (up to 14wt%Bi) do not form (Bi) phase in their equilibrium solidification path. However, non-equilibrium βSn +$(Cu,Ni)_6Sn_5$+(Bi) eutectic formed due to the limited backdiffusion of Bi within βSn for all joints with Bi contents ≥2wt% Bi, when cooled at 3K/s.

Acknowledgements

This research was funded by Nihon Superior Co., Ltd. and EPSRC grant no. EP/M002241/1

References

[1] R. Schueller, N. Blattau, J. Arnold, and C. Hillman, Second generation Pb-free alloys, J SMTA, 23 (2010) 18-26.

[2] M. Laentzsch, Theory and practical experience of micro-alloyed SnCu0.7NiGe (SN100C). 2006 Electronics Systemintegration Technology Conference, New York: IEEE.

[3] V. Vuorinen, H. Yu, T. Laurila, and J.K. Kivilahti, Formation of Intermetallic Compounds Between Liquid Sn and Various CuNi x Metallizations, J Electron Mater, 37 (2008)792-805.

[4] L. Snugovsky, P. Snugovsky, D.D. Perovic, and J. W. Rutter, Phase equilibria in Sn rich corner of Cu–Ni–Sn system, Mater Sci Technol, 22 (2008) 899-902.

[5] C.M. Gourlay, K. Nogita, J. Read, and A. K. Dahle, Intermetallic Formation and Fluidity in Sn-Rich Sn-Cu-Ni Alloys, J Electron Mater, 39 (2010) 56-69.

[6] T. Ventura, C.M. Gourlay, K. Nogita, T. Nishimura, M. Rappaz, and A. K. Dahle, The Influence of 0–0.1 wt.% Ni on the Microstructure and Fluidity Length of Sn-0.7Cu-xNi, J Electron Mater, 37 (2008) 32-39.

[7] C.M. Gourlay, J. Read, K. Nogita, and A.K. Dahle, The maximum fluidity length of solidifying Sn-Cu-Ag-Ni solder alloys, J Electron Mater, vol. 37 (2008) 51-60.

[8] C.Y. Huang, H.H. Huang, and K.C. Ying, Sn-Cu-Ni soldering process optimization using multivariate analysis, IEEE Transactions on Components, Packaging and Manufacturing Technology, vol. 2 (2012) 527-535.

[9] K. Nogita and T. Nishimura, Nickel-stabilized hexagonal (Cu, $Ni)_6Sn_5$ in Sn-Cu-Ni lead-free solder alloys, Scripta Mater, 59 (2008) 191-194.

[10] U. Schwingenschlogl, C. Di Paola, K. Nogita, and C.M. Gourlay, The influence of Ni additions on the relative stability of eta and eta(') Cu6Sn5, Appl Phys Lett, 96 (2010) 1-3.

[11] C. Yang, F. Song, and S.W. Ricky Lee, Impact of Ni concentration on the intermetallic compound formation and brittle fracture strength of Sn–Cu–Ni (SCN) lead-free solder joints, Microelectron Reliab, 54 (2014) 435-446.

[12] H. Nishikawa, J.Y. Piao, and T. Takemoto, Interfacial reaction between Sn-0.7Cu(-Ni) solder and Cu substrate, J Electron Mater, 35 (2006) 1127-1132.

[13] J.W. Yoon, Y.H. Lee, D.G. Kim, H.B. Kang, S.J. Suh, C.W. Yang, et al., Intermetallic compound layer growth at the interface between Sn-Cu-Ni solder and Cu substrate, J Alloy Compd, 381 (2004) 151-157.

[14] M.J. Rizvi, C. Bailey, Y.C. Chan, M.N. Islam and H. Lu, Effect of adding 0.3 wt% Ni into the Sn-0.7 wt% Cu solder: Part II. Growth of intermetallic layer with Cu during wetting and aging, J Alloy Compd, 438 (2007) 122-128.

[15] T. Laurila, J. Hurtig, V. Vuorinen, and J.K. Kivilahti, Effect of Ag, Fe, Au and Ni on the growth kinetics of Sn-Cu intermetallic compound layers, Microelectron Reliab, 49 (2009) 242-247.

[16] Y.W. Wang, Y.W. Lin, C.T. Tu, and C.R. Kao, Effects of minor Fe, Co, and Ni additions on the reaction between SnAgCu solder and Cu, J Alloy Compd, 478 (2009) 121-127.

[17] M.A.A. Mohd Salleh, S.D. McDonald, C.M. Gourlay, S.A. Belyakov, H.Yasuda, and K.Nogita, Effect of Ni on the Formation and Growth of Primary Cu6Sn5 Intermetallics in Sn-0.7 wt.%Cu Solder Pastes on Cu Substrates During the Soldering Process, J Electron Mater, 45 (2015)154-163.

[18] H. Tsukamoto, T. Nishimura, S. Suenaga, S.D. McDonald, K.W. Sweatman, and K. Nogita, The influence of solder composition on the impact strength of lead-free solder ball grid array joints, Microelectron Reliab, 51 (2011) 657-667.

[19] J. Johansson, I. Belov, E. Johnson, R. Dudek, and P. Leisner, Investigation on thermal fatigue of SnAgCu, Sn100C, and SnPbAg solder joints in varying temperature environments, Microelectron Reliab, 54 (2014) 2523-2535.

[20] J. Arnold, N. Blattau, C. Hillman, D. Solutions, and K. Sweatman, Reliability Testing of Ni-Modified SnCu and SAC305, Accelerated Thermal Cycling, Resistor, 1 (2008) 1.

[21] J. Nguyen, Assembly Process Feasibility of Low/No Silver Alloy Solder Paste Materials, IPC APEX EXPO, Las Vegas , NV, 2008.

[22] E. George, M. Osterman, and M. Pecht, An evaluation of dwell time and mean cyclic temperature parameters in the Engelmaier model, Microelectron Reliab, 55 (2015) 582-587.
[23] R.J. Coyle, K. Sweatman, and B. Arfaei, Thermal Fatigue Evaluation of Pb-Free Solder Joints: Results, Lessons Learned, and Future Trends, JOM, 67 (2015) 2394-2415.
[24] R. Parker, Coyle, R., Henshall, G., Smetana, J., and E. Benedetto, Pb-Free Alloy Characterization Project Report: Part II–Thermal Fatigue Results for Two Common Temperature Cycles, SMTAI 2012, Orlando, FL, (2012) 348-358.
[25] P.T. Vianco and J.A. Rejent, Properties of ternary Sn-Ag-Bi solder alloys: Part I - Thermal properties and microstructural analysis, J Electron Mater, 28 (1999) 1127-1137.
[26] Y. Liu, F.L. Sun, Y. Liu, and X.M. Li, Effect of Ni, Bi concentration on the microstructure and shear behavior of low-Ag SAC-Bi-Ni/Cu solder joints, J Mater Sci - Mater Electron, 25 (2014) 2627-2633.
[27] J. Shen, Y.Y. Pu, D. Wu, Q. Tang, and M.L. Zhao, Effects of minor Bi, Ni on the wetting properties, microstructures, and shear properties of Sn-0.7Cu lead-free solder joints, J Mater Sci - Mater Electron, 26 (2015) 1572-1580.
[28] J. Zhao, L. Qi, X.M. Wang, and L.Wang, Influence of Bi on microstructures evolution and mechanical properties in Sn-Ag-Cu lead-free solder, J Alloy Compd, 375 (2004) 196-201.
[29] R. Pandher and R. Healey, Reliability of Pb-free solder alloys in demanding BGA and CSP applications, 58th Electronic Components & Technology Conference, New York: IEEE (2008) 2018-2023.
[30] J. Zhao, Y. Mutoh, Y. Miyashita, and S.L. Mannan, Fatigue crack-growth behavior of Sn-Ag-Cu and Sn-Ag-Cu-Bi lead-free solders, J Electron Mater, 31 (2002) 879-886.
[31] Y. Mutoh, J. Zhao, Y. Miyashita, and C. Kanchanomai, Fatigue crack growth behaviour of lead-containing and lead-free solders, Solder Surface Mount Technol, 14 (2002) 37-45.
[32] J. Zhao, C.Q. Cheng, L. Qi, and C.Y. Chi, Kinetics of intermetallic compound layers and shear strength in Bi-bearing SnAgCu/Cu soldering couples, J Alloy and Compd, 473 (2009) 382-388.
[33] P. T. Vianco and J.A. Rejent, Properties of ternary Sn-Ag-Bi solder allays: Part II - Wettability and mechanical properties analyses, J Electron Mater, 28 (1999) 1138-1143.
[34] Y. Liu, F. Sun, and X. Liu, Improving Sn-0.3Ag-0.7Cu low-Ag lead-free solder performance by adding Bi element, Strategic Technology (IFOST), International Forum, (2010) 343-346.
[35] E. Hodulova, M. Palcut, E. Lechovic, B. Simekova, and K. Ulrich, Kinetics of intermetallic phase formation at the interface of Sn-Ag-Cu-X (X = Bi, In) solders with Cu substrate, J Alloy Compd, 509 (2011) 7052-7059.
[36] M. He and V.L. Acoff, Effect of Bi on the interfacial reaction between Sn-3.7Ag-xBi solders and Cu," J Electron Mater, 37 (2008) 288-299.
[37] K.S. Kim, C.H. Yu, and J.M. Yang, Behavior of tin whisker formation and growth on lead-free solder finish, Thin Solid Films, 504 (2006) 350-354.
[38] P. Zhang, Y. Zhang, and Z. Sun, Spontaneous Growth of Metal Whiskers on Surfaces of Solids: A Review, J Mater Sci Technol, 31 (2015) 675-698.
[39] K.W. Moon, W.J. Boettinger, U.R. Kattner, F.S. Biancaniello, and C.A. Handwerker, Experimental and thermodynamic assessment of Sn-Ag-Cu solder alloys, J Electron Mater, 29 (2000) 1122-1136.
[40] R.I. Wu and J.H. Perepezko, Liquidus temperature determination in multicomponent alloys by thermal analysis, Metallurg Mater Trans A, 31 (2000) 497-501.
[41] W.J. Boettinger, U.R. Kattner, K.W. Moon, and J.H. Perepezko, Chapter five - DTA and heat flux DSC measurements of alloy melting and freezing, Methods for Phase Diagram Determination, ed Oxford: Elsevier Science Ltd, 2007.
[42] Phase Diagrams & Computational Thermodynamics
http://www.metallurgy.nist.gov/phase/solder/bisn.html
[43] Thermo-Calc. TCSLD Database version 3.1 (2015) [Online].
[44] C.M. Gourlay, K.Nogita, A.K. Dahle, Y. Yamamoto, K. Uesugi, T. Nagira, et al., In situ investigation of unidirectional solidification in Sn–0.7Cu and Sn–0.7Cu–0.06Ni, Acta Mater, 59 (2011) 4043-4054.

[45] K. Nogita, C.M. Gourlay, and T. Nishimura, Cracking and phase stability in reaction layers between Sn-Cu-Ni solders and Cu substrates, JOM, 61 (2009) 45-51.
[46] R. Gagliano and M.E. Fine, Growth of η phase scallops and whiskers in liquid tin-solid copper reaction couples, JOM, 53 (2001) 33-38.
[47] Y. Tian, R. Zhang, C. Hang, L. Niu, and C. Wang, Relationship between morphologies and orientations of Cu6Sn5 grains in Sn3.0Ag0.5Cu solder joints on different Cu pads, Mater Charact, 88 (2014) 58-68.
[48] M.Y. Li, Z.H. Zhang, and J.M. Kim, Polymorphic transformation mechanism of η and η' in single crystalline Cu6Sn5, Appl Phys Lett, 98 (2011) 201901.
[49] Z.H. Zhang, H.J. Cao, H.F. Yang, M.Y. Li, and Y.X. Yu, Hexagonal-Rod Growth Mechanism and Kinetics of the Primary Cu6Sn5 Phase in Liquid Sn-Based Solder, J Electron Mater, 45 (2016) 5985-5995.
[50] J.W. Xian, S.A. Belyakov, and C.M. Gourlay, Controlling Bulk Cu6Sn5 Nucleation in Sn0.7Cu/Cu Joints with Al Micro-alloying, J Electron Mater, 45 (2015) 69-78.
[51] Y.Q. Wu, S.D. McDonald, J.Read, H.Huang, and K.Nogita, Determination of the minimum Ni concentration to prevent the η to η4+1 polymorphic transformation of stoichiometric Cu6Sn5, Scripta Mater, 68 (2013) 595-598.
[52] C.M. Gourlay, S.A. Belyakov, Z.L. Ma, and J.W. Xian, Nucleation and Growth of Tin in Pb-Free Solder Joints, JOM, (2015) 1-11.
[53] A. Ohno and T. Motegi, The Effect of Small Additives on the Undercooling of Pure Tin, J. Japan Inst Metal (1973) 777 -780.
[54] S.K. Kang, M.G. Cho, P.Lauro, D.Y. Shih, Critical factors affecting the undercooling of Pb-free, flip-chip solder bumps and in-situ observation of solidification process, 57th Electronic Components & Technology Conference, New York: IEEE, 2007.
[55] L.W. Lin, J.M. Song, Y.S. Lai, Y.T. Chiu, N.C. Lee, and J.Y. Uan, Alloying modification of Sn-Ag-Cu solders by manganese and titanium, Microelectron Reliab, 49 (2009) 235-241.
[56] S.A. Belyakov and C.M. Gourlay, Heterogeneous nucleation of beta Sn on NiSn4, PdSn4 and PtSn4, Acta Mater, 71 (2014) pp. 56-68.
[57] Z.L. Ma, S.A. Belyakov, and C.M. Gourlay, Effects of cobalt on the nucleation and grain refinement of Sn-3Ag-0.5Cu solders, J Alloy Compd, 682 (2016) 326-337.
[58] G. Parks, A. Faucett, C. Fox, J. Smith, and E. Cotts, The Nucleation of Sn in Undercooled Melts: The Effect of Metal Impurities, JOM, 66 (2014) 2311-2319.
[59] Y.C. Huang, S.W. Chen, and K.S. Wu, Size and Substrate Effects upon Undercooling of Pb-Free Solders, J Electron Mater, 39 (2010) 109-114.
[60] M.G. Cho, S.K. Kang, and H.M. Lee, Undercooling and microhardness of Pb-free solders on various under bump metallurgies, J Mater Res, 23 (2008), 1147-1154.
[61] J.W. Xian, Z.L. Ma, S.A. Belyakov, M. Ollivier, C.M. Gourlay, Nucleation of tin on the Cu6Sn5 layer in electronic interconnections, Acta Mater, 123 (2017) 404-415.
[62] A.U. Telang and T.R. Bieler, The orientation imaging microscopy of lead-free Sn-Ag solder joints, JOM, 57 (2005) 44-49.
[63] L.P. Lehman, Y. Xing, T.R. Bieler, and E.J. Cotts, Cyclic twin nucleation in tin-based solder alloys, Acta Mater, 58 (2010) 3546-3556.
[64] B. Arfaei, N. Kim, and E.J. Cotts, Dependence of Sn Grain Morphology of Sn-Ag-Cu Solder on Solidification Temperature, J Electron Mater, 41 (2012) 362-374.
[65] B. Arfaei and E. Cotts, Correlations Between the Microstructure and Fatigue Life of Near-Eutectic Sn-Ag-Cu Pb-Free Solders, J Electron Mater, 38 (2009) 2617-2627.
[66] P. Darbandi, T.R. Bieler, F. Pourboghrat, and T.K. Lee, The Effect of Cooling Rate on Grain Orientation and Misorientation Microstructure of SAC105 Solder Joints Before and After Impact Drop Tests, J Electron Mater, 43 (2014) 2521-2529.
[67] A. Mayyas, A. Qasaimeh, P. Borgesen, and M. Meilunas, Effects of latent damage of recrystallization on lead free solder joints, Microelectron Reliab, 54 (2014) 447-456.

[68] T.K. Lee, B. Zhou, L. Blair, K.C. Liu, and T.R. Bieler, Sn-Ag-Cu Solder Joint Microstructure and Orientation Evolution as a Function of Position and Thermal Cycles in Ball Grid Arrays Using Orientation Imaging Microscopy, J Electron Mater, 39 (2010) 2588-2597.
[69] T.C. Huang, T.L. Yang, J.H. Ke, C.H. Hsueh, and C.R. Kao, Effects of Sn grain orientation on substrate dissolution and intermetallic precipitation in solder joints under electron current stressing, Scripta Mater, 80 (2014) 37-40.
[70] M. Lu, D.Y. Shih, P. Lauro, C. Goldsmith, and D.W. Henderson, Effect of Sn grain orientation on electromigration degradation mechanism in high Sn-based Pb-free solders, Appl Phy Lett, 92 (2008) 211909.
[71] T.K. Lee, T.R. Bieler, C.U. Kim, and H. Ma, Fundamentals of Lead-Free Solder Interconnect Technology, 1 ed.: Springer US, 2015.
[72] M.H. Mahdavifard, M.F.M. Sabri, S.M. Said, D.A. Shnawah, I.A. Badruddin, and S.Rozali, Effects of Fe and Bi Minor Alloying on Mechanical, Thermal, and Microstructural Properties of Sn-0.7Cu Solder Alloy, J Electron Mater, 45 (2010) 3673-3682.

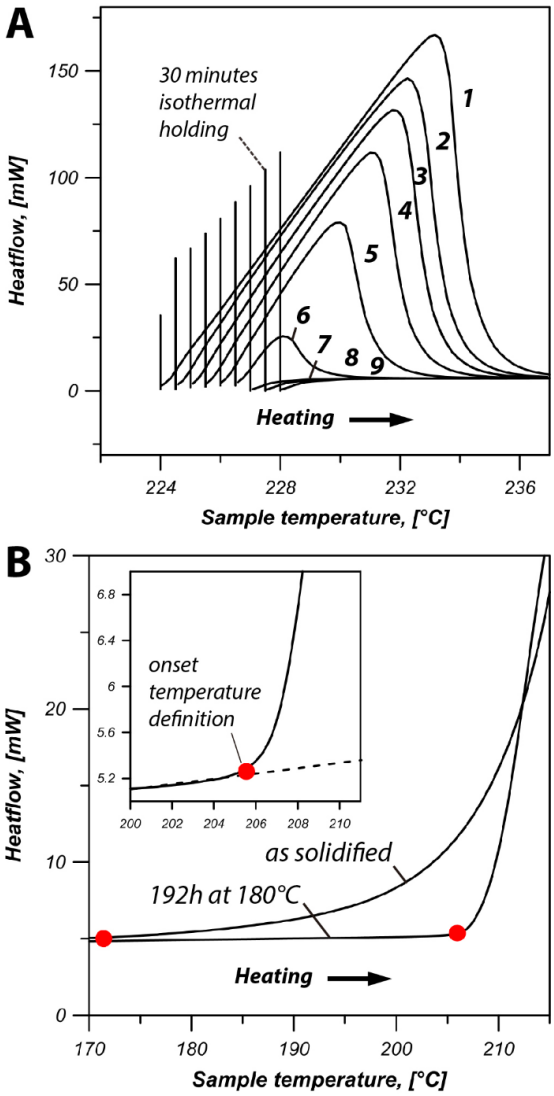

Figure 1. (A): Cyclic DSC method for the determination of the liquidus temperature. The number next to the heating curve reflects the number of the cycle. Isothermal holding temperature step is 0.5K; (B) Typical DSC heating curves showing the influence of homogenization (192h at 180°C) on the onset of the endothermic reaction.

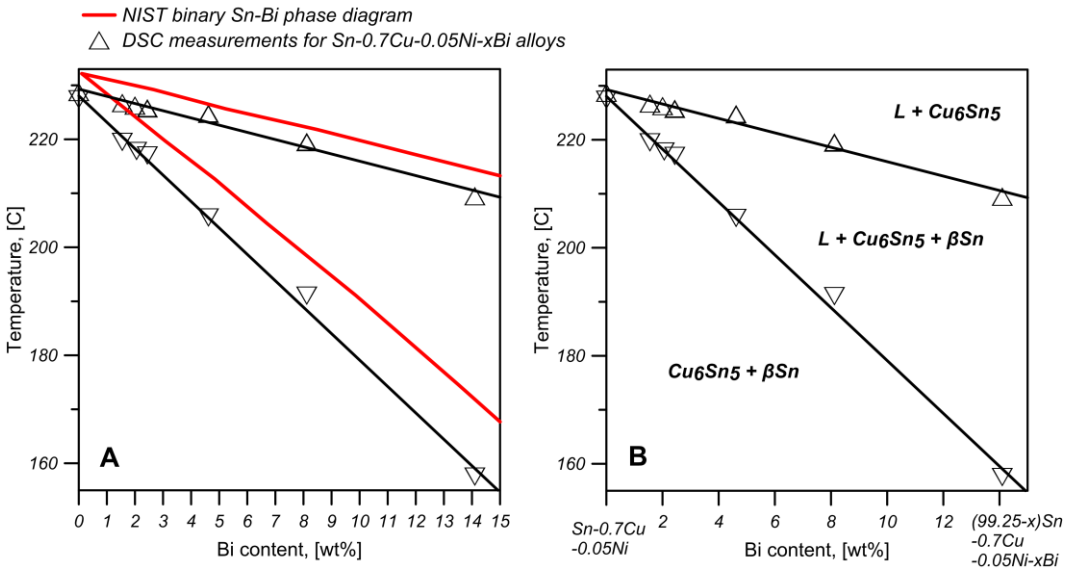

Figure 2. (A): DSC measurements of the 'liquidus' and solidus temperatures of Sn-0.7Cu-0.05Ni-xBi alloys shown as triangles. NIST data [42] for the binary Sn-Bi system is shown as red lines. (B): vertical section through (99.25-x)Sn-0.7Cu-0.05Ni-xBi with phase fields denoted based on Figures 2A and 3.

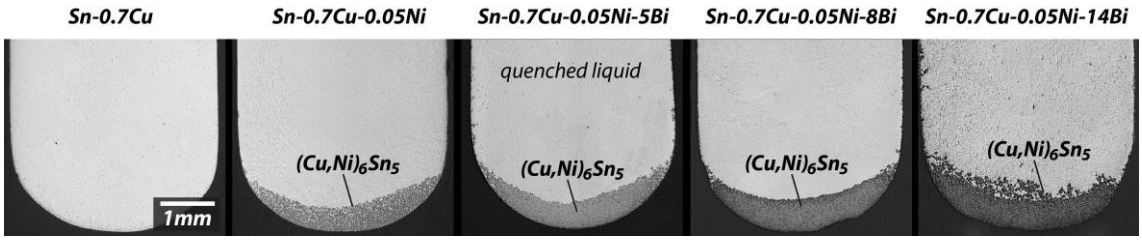

Figure 3. Bottom parts of quenched samples held in quartz tubes during isothermal holding experiments (192h at 250°C) featuring settled layers of $(Cu,Ni)_6Sn_5$ crystals.

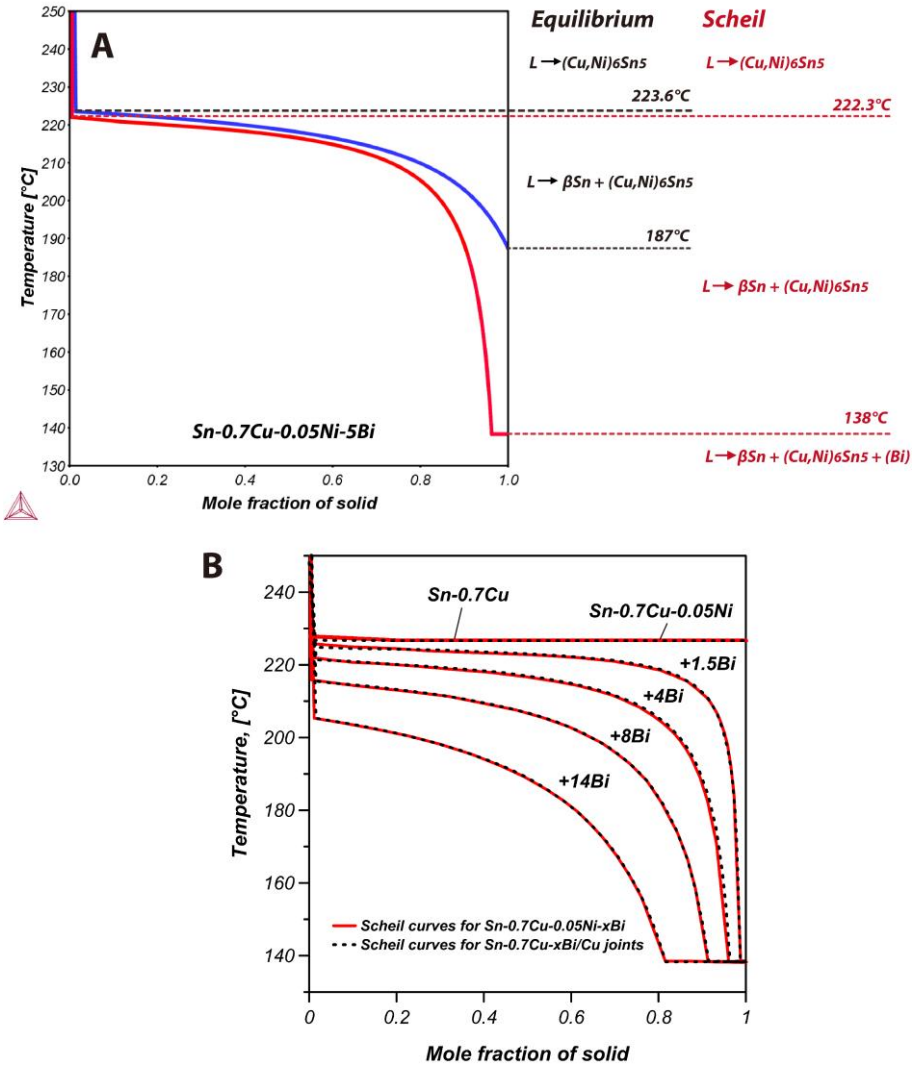

Figure 4. (A): Equilibrium and Scheil solidification sequences in Sn-0.7Cu-0.05Ni-5Bi; (B): Scheil solidification sequences in Sn-0.7Cu-0.05Ni-xBi solders and Sn-0.7Cu-xBi/Cu solder joints. (A-B): as predicted by ThermoCalc TCSLD 3.1;

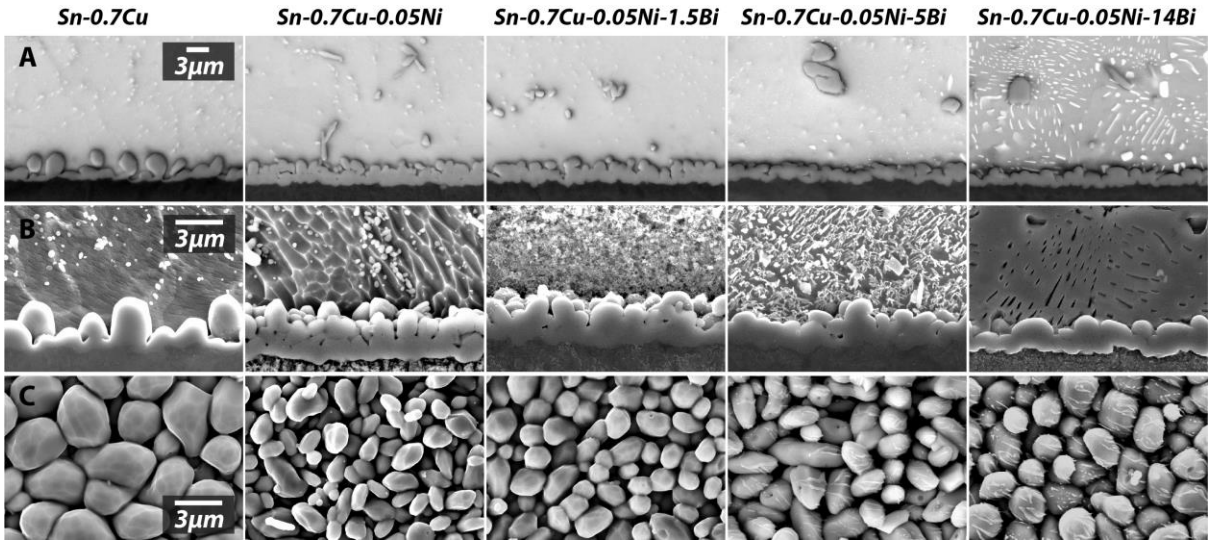

Figure 5. Typical BSE and SEM micrographs of interfacial IMC layers in Sn-0.7Cu and Sn-0.7Cu-0.05Ni-xBi solder joints. Row (A): BSE micrographs of interfacial IMC layers, vertical cross-section; row (B): areas similar to (A) after selective etching of βSn and row (C): SEM micrographs of interfacial IMC layers after removal of βSn, view from above. Each row has the same magnification. Peak reflow temperature 251°C.

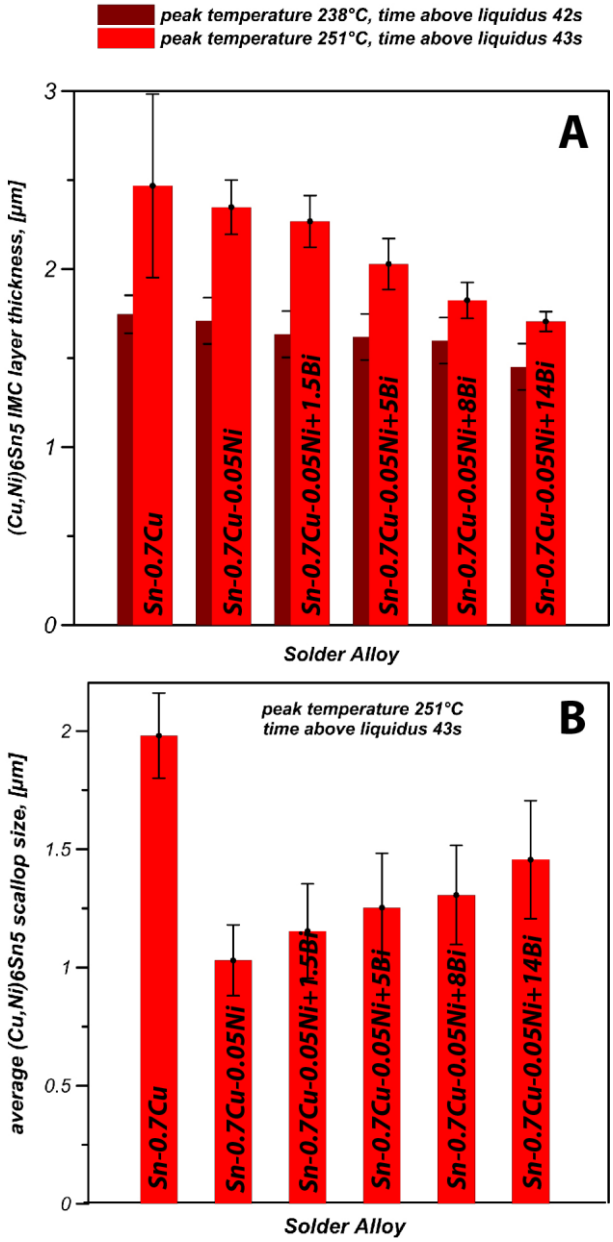

Figure 6. (A): Influence of Bi additions on the thickness and (B): on the average $(Cu,Ni)_6Sn_5$ grain size in the IMC layer in Sn-0.7Cu/Cu and Sn-0.7Cu-0.05Ni-xBi/Cu solder joints.

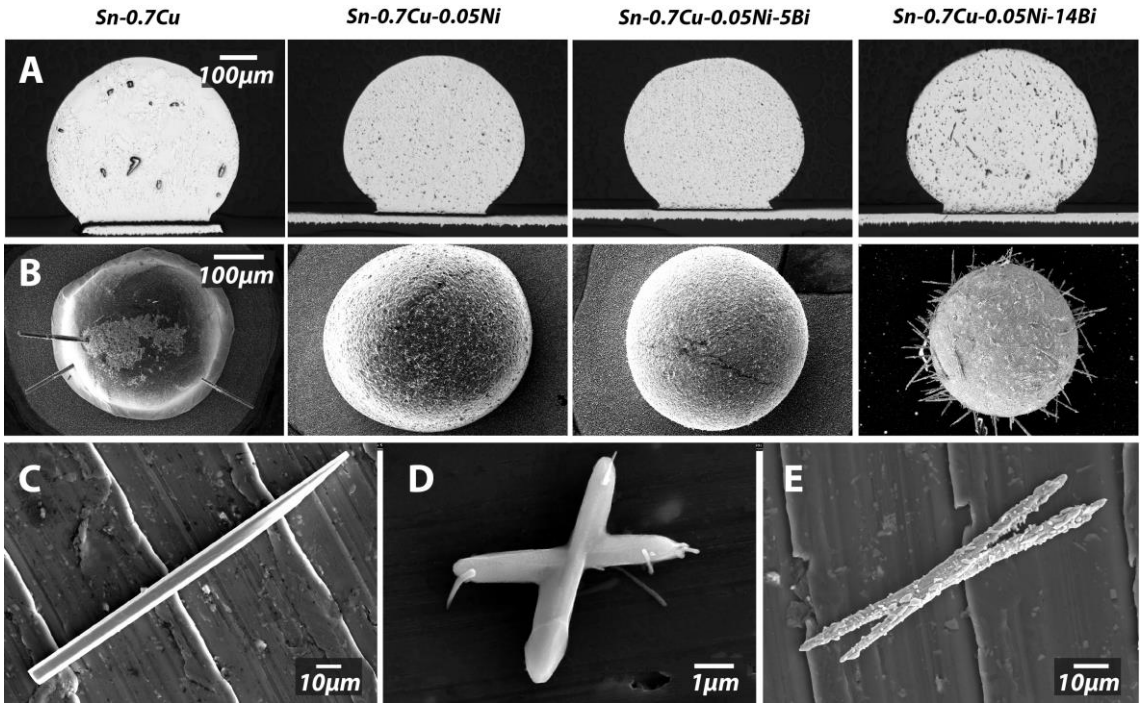

Figure 7. (A-B): Typical cross sections of Sn-0.7Cu/Cu and Sn-0.7Cu-0.05Ni-xBi/Cu solder joints. (A) OM cross-sections. (B): SEM images of etched joints showing the primary $(Cu,Ni)_6Sn_5$ crystals formed in the bulk. Primary $(Cu,Ni)_6Sn_5$ are too small to be resolved at this magnification in Sn-0.7Cu-0.05Ni and Sn-0.7Cu-0.05Ni +4.6Bi samples. (C-E): Typical examples of primary $(Cu,Ni)_6Sn_5$ crystals formed in (C): Sn-0.7Cu/Cu, (D) Sn-0.7Cu-0.05Ni/Cu and (E): Sn-0.7Cu-0.05Ni-14.1Bi/Cu solder joints. Note the different scale bars.

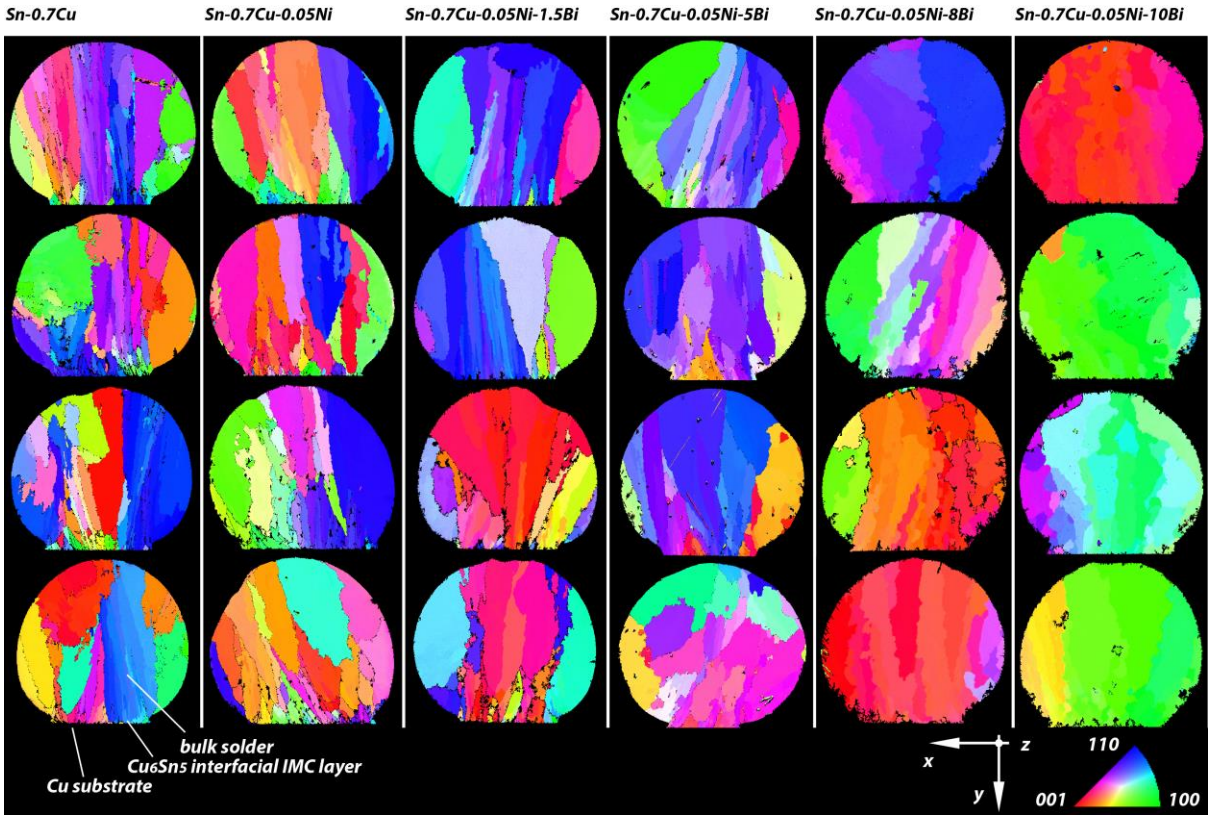

Figure 8. Representative βSn grain structures. EBSD IPFX maps for Sn-0.7Cu/Cu and Sn-0.7Cu-0.05Ni-xBi/Cu solder joints.

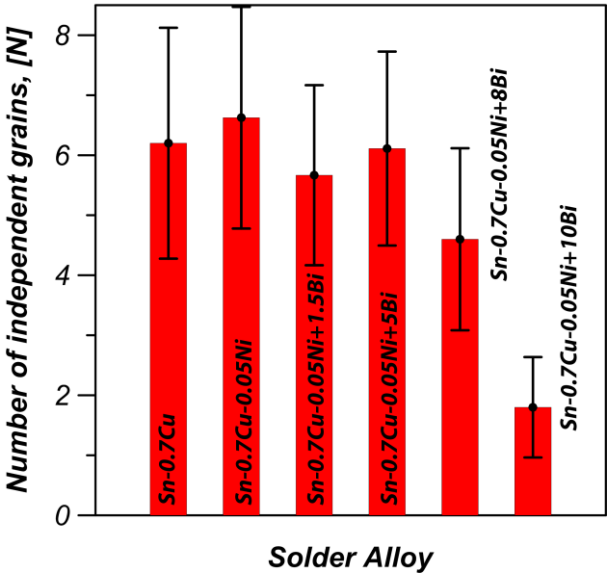

Figure 9. Summary of the number of independent βSn grains for each investigated Sn-0.7Cu-0.05Ni-xBi/Cu solder joint combination.

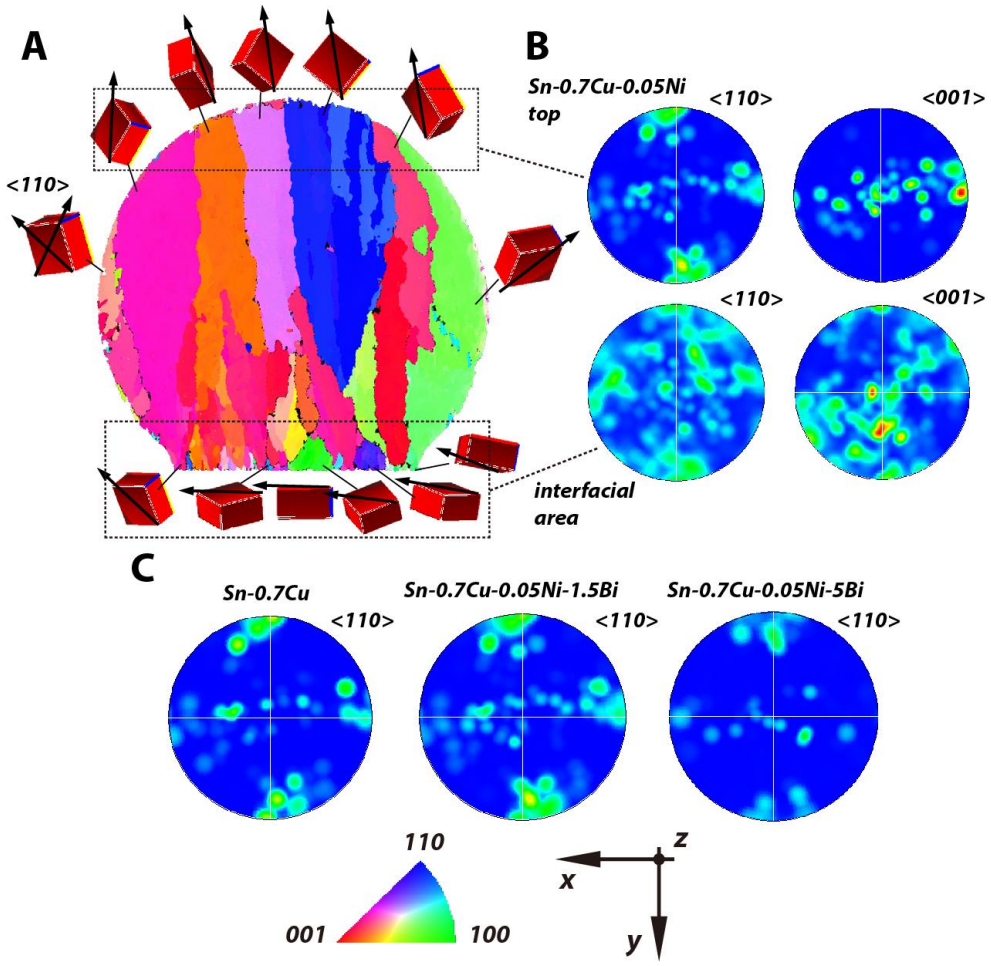

Figure 10. (A): representative βSn grain structure formed in Sn-0.7Cu-0.05Ni/Cu solder joints (EBSD IPFX map) with 13 unit cell orientations superimposed; (B) and (C): <110> and <001> cumulative pole figures of the βSn grain orientations in the upper and interfacial parts of solder joints. Compositions are labelled above each pole figure. Each pole figure is a compilation data from 10 individual solder joints for each composition.

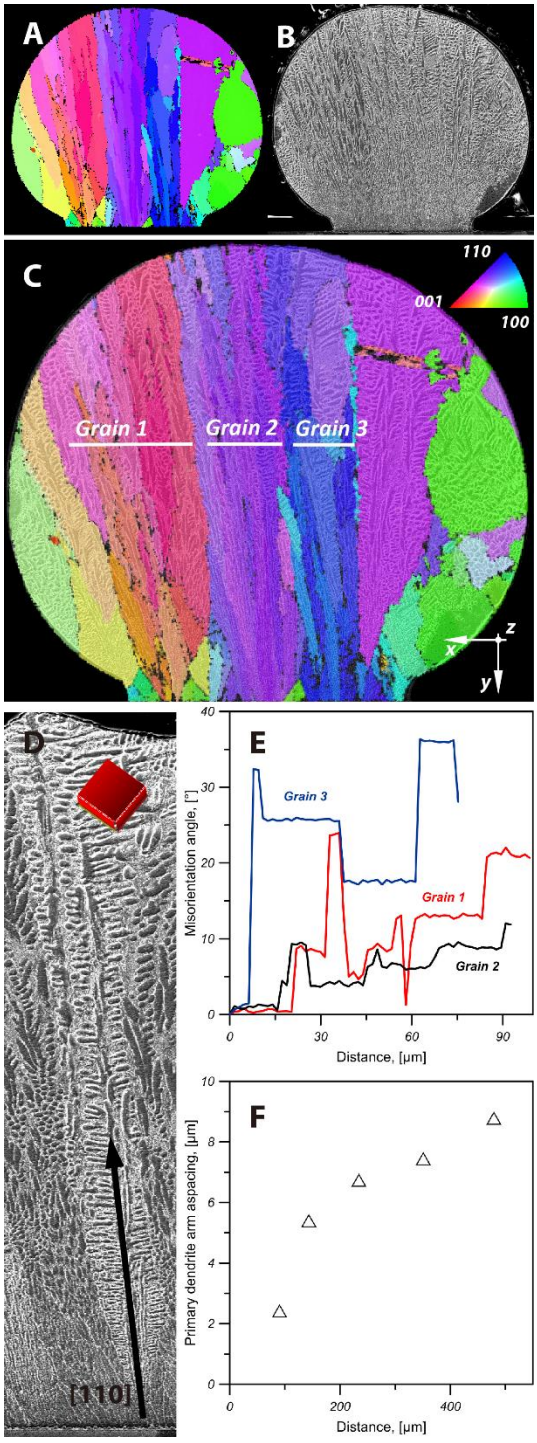

Figure 11. (A): representative EBSD IPFX map of a Sn-0.7Cu/Cu solder joint; (B): the joint in (A) after shallow etching; (C): overlapped (A) and (B) images; (D) typical example of a βSn dendrite nucleated at the solder/IMC layer interface (after shallow etching); (E): misorientation profile of the grains labelled in (C); (F): plot of secondary dendrite arm spacing as a function of the distance from the solder/IMC layer interface in (D).

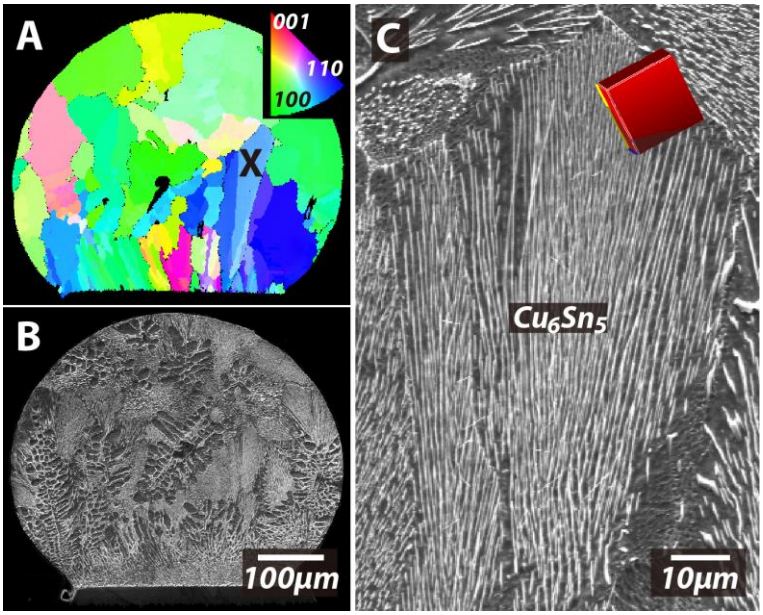

Figure 12. βSn-Cu_6Sn_5 eutectic grain in a Sn0.7Cu/Cu joint. (A): EBSD IPFX map; (B): solder joint in (A) after shallow etching, containing eutectic grains and βSn dendrites; (C): Cu_6Sn_5 rods in the 'blue' βSn-Cu_6Sn_5 eutectic grain labelled 'X' in (A). βSn unit cell orientation is superimposed.

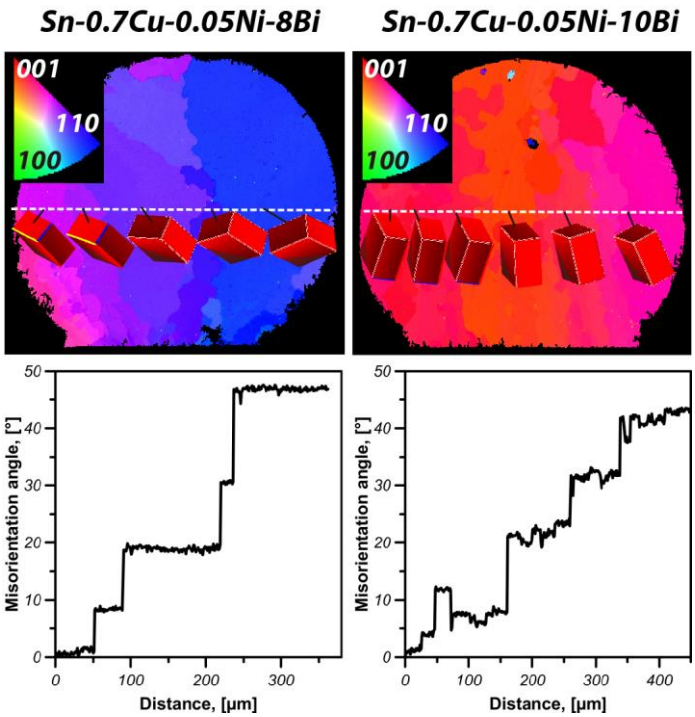

Figure 13. Representative examples of EBSD IPFX maps for Sn-0.7Cu-0.05Ni-8Bi/Cu and Sn-0.7Cu-0.05Ni-10Bi/Cu solder joints and corresponding misorientation profiles. βSn unit cell orientation is superimposed.

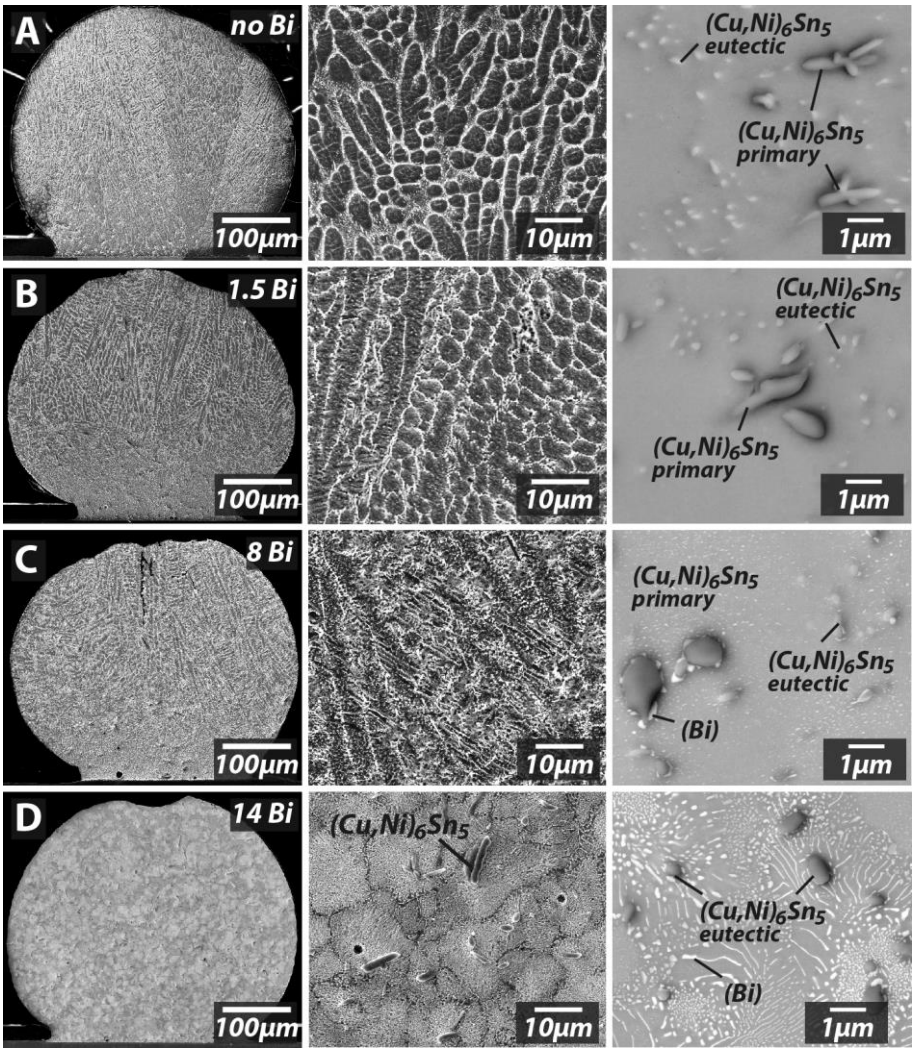

Figure 14. Typical microstructures of Sn-0.7Cu-0.05Ni-xBi/Cu solder joints shown at two magnifications after shallow etching. (A)-(D) are 0, 1.5, 4, 8 and 14wt%Bi respectively.

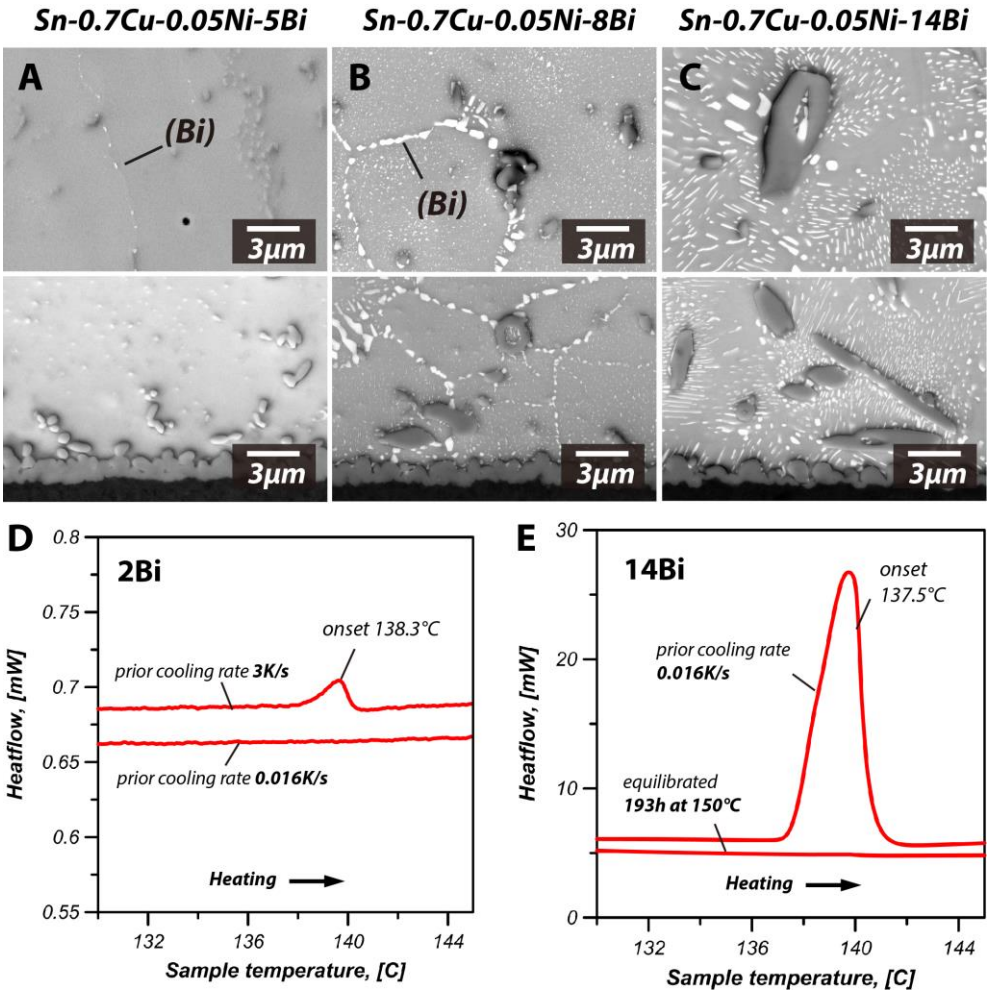

Figure 15. (A-C): Typical examples of non-equilibrium Sn-$(Cu,Ni)_6Sn_5$-(Bi) eutectic in the solder joint bulk and at the interface at three Bi levels; (D): DSC heating curves for Sn-0.7Cu-0.05Ni-2Bi alloy demonstrating formation nonequilibrium Sn-$(Cu,Ni)_6Sn_5$-(Bi) eutectic at cooling rates of 3K/s; (E): DSC heating curves for Sn-0.7Cu-0.05Ni-14Bi alloy demonstrating presence of some nonequilibrium Sn-$(Cu,Ni)_6Sn_5$-(Bi) eutectic at cooling rates of 0.016K/s that disappears after heat treatment for 193hours at 150°C.

Table 1. Compositions in wt%, as determined by ICP-AES. Detected levels of Cd, Al, Zn and Ag were <0.001 wt%.

Nominal composition	**Cu**, wt%	**Ni**, t%	**Bi**, wt%	**Pb**, wt%	**Ag**, wt%	**Sb**, wt%	**Fe**, wt%	**As**, wt%
Sn-0.7Cu	0.693	0.002	＜0.001	0.004	0.017	0.021	0.004	＜0.001
Sn-0.7Cu-0.05Ni	0.678	0.041	＜0.001	0.005	0.010	0.017	0.002	＜0.001
Sn-0.7Cu-0.05Ni-1.5Bi	0.669	0.043	1.55	＜0.001	0.013	0.019	0.003	0.014
Sn-0.7Cu-0.05Ni-2Bi	0.667	0.043	2.06	＜0.001	0.009	0.020	0.003	0.021
Sn-0.7Cu-0.05Ni-5Bi	0.658	0.042	4.62	＜0.001	0.007	0.012	0.003	0.054
Sn-0.7Cu-0.05Ni-8Bi	0.721	0.039	8.12	＜0.001	0.001	0.011	0.004	0.137
Sn-0.7Cu-0.05Ni-10Bi	0.697	0.046	9.7	＜0.001	＜0.001	0.004	0.004	0.154
Sn-0.7Cu-0.05Ni-14Bi	0.739	0.043	14.1	＜0.001	＜0.001	0.003	0.003	0.006

Table 2. Measured equilibrium temperatures in Sn-0.7Cu-0.05Ni-xBi alloys. 'Liquidus' temperatures are βSn-Cu_6Sn_5 eutectic start temperatures in Figure 2B.

Sn-0.7Cu-0.05Ni+	***0Bi***	***1.5Bi***	***2Bi***	***2.4Bi***	***4.6Bi***	***8.1Bi***	***14.1Bi***
'Liquidus' temperature, °C	228.75	226.75	226.25	225.75	224.75	219.5	209.5
Solidus temperature, °C	227.4 (0.2)	219.5 (0.4)	217.8 (0.6)	217.0 (0.6)	205.5 (0.8)	192.0 (1.1)	164.5 (1.3)

Please note, the accuracy of the liquidus temperature determination was 0.25K. Standard deviation for solidus temperature measurements is shown in brackets

Table 3. SEM-EDX results for the $(Cu,Ni)_6Sn_5$ crystals from the settled layers in Figure 3. The Bi content in $(Cu,Ni)_6Sn_5$ was below the resolution limit for all compositions.

Alloy composition	***Number of particles studied***	***Ni, at%***	***Cu, at%***	***Sn, at%***
Sn-0.7Cu-0.05Ni	22	16.6 (1.9)	39.1 (1.9)	44.3 (2.5)
Sn-0.7Cu-0.05Ni-**5Bi**	19	14.4 (2.1)	41.6 (2.5)	44.0 (2.3)
Sn-0.7Cu-0.05Ni-**8Bi**	15	9.7 (1.8)	46.8 (2.3)	43.5 (1.8)
Sn-0.7Cu-0.05Ni-**14Bi**	16	8.2 (2.0)	47.9 (2.1)	43.9 (1.6)

Mean compositions are shown with standard deviation in brackets

Table 4. Typical SEM-EDX results for the $(Cu,Ni)_6Sn_5$ crystals formed in interfacial IMC layers and in the solder bulk (primary IMCs). The Bi content in $(Cu,Ni)_6Sn_5$ was always below the resolution limit.

Alloy composition	***Number of particles studied***	***Ni, at%***	***Cu, at%***	***Sn, at%***
	Interfacial IMC layer			
Sn-0.7Cu	10	-	57.9 (1.8)	42.1 (1.9)
Sn-0.7Cu-0.05Ni	10	3.0 (2.6)	54.1 (2.5)	42.9 (1.4)
Sn-0.7Cu-0.05Ni-**1.5Bi**	12	2.4 (1.6)	55.2 (2.3)	42.4 (1.6)
Sn-0.7Cu-0.05Ni-**14Bi**	9	2.2 (2.1)	57.0 (1.8)	40.8 (1.2)
	Bulk primary IMCs			
Sn-0.7Cu	10	-	56.7 (2.0)	43.3 (2.1)
Sn-0.7Cu-0.05Ni	9	8.0 (3.9)	49.2 (2.8)	42.8 (1.8)
Sn-.7Cu-0.05Ni-**1.5Bi**	10	5.8 (2.6)	50.8 (2.7)	43.4 (1.4)
Sn-0.7Cu-0.05Ni-**14Bi**	11	5.4 (3.1)	51.0 (3.3)	43.6 (2.4)
Mean compositions are shown with standard deviation in brackets				